Characterizing spectral diffusion in V^{4+} doped 4H-SiC

Physics BSc Thesis

Michael Bruno

Student Number: S3981541

First Supervisor: prof. dr. ir. C.H. van der Wal

Second Examiner: prof. dr. G. Palasantzas

Daily Supervisor: J. Hendriks MSc

Research Group: Physics of Quantum Devices

Zernike Institute for Advanced Materials

FSE

Rijksuniversiteit Groningen

6 July 2022

Abstract

This paper attempts to uncover more information on the phenomena of spectral diffusion occurring within a V^{4+} doped 4H-SiC sample. A model was developed in python in order to study the fluctuations in the number of defects that could absorb a laser light with a specific wavelength at each point in time. Different spectral diffusion speeds were compared, but no difference was found over the timescales used. In parallel with the modelling, an experiment was carried out where comparisons were made between signals arising from the laser light only and the signal resulting from absorption of the light by the SiC sample situated within a cryostat. The peaks found comparing the two signals were at identical frequencies, but a clear heightening of the signal noise floor was observed when the laser passed through the sample. This difference disappeared at room temperature and was found to increase with increasing laser power. This suggests some temperature dependent interactions occurring, but is likely not due to vanadium defects as the difference also appears when using laser light off resonance.

Dedication

To my Mom, Dad and Sister

Acknowledgements

I want to thank the 'Physics of Quantum Devices' research group for taking me in and teaching me a bunch of cool new things and most importantly my daily supervisor Joop Hendriks who guided me every step of the way.

A big thank you to the other students in the office space that engaged in mutual distraction with me to occasionally take my mind off work worries, but who also tried to help me out whenever I was unsure about something.

I also want to thank my family for their support throughout my entire bachelors degree as well as all my friends who have helped me stay on track and have fun throughout it.

Contents

Chapter 1

Introduction

Applications of quantum technologies are a rapidly growing area of research, with applications such as quantum key distribution already being used today [1]. In order to construct real-world quantum communication networks, more research needs to be conducted in the related quantum technological areas. One of these is quantum memory, where multiple quantum systems have found their advantages and disadvantages in contributing to this research. The most studied among these are trapped ions, semiconductor quantum dots, and solid-state color centers, all of which store the quantum information in the spin of charged particles [2]. One candidate in the color center group is the semiconductor silicon carbide (SiC). It is very robust and has a wide band gap that allows light of most wavelengths around the visible and near infra red ranges to pass through it without absorption. This thesis focuses on the use of Vanadium defects within SiC. These defects are optically active in the telecom wavelengths, a unique feature of vanadium, which allows for simpler integration with already existing communication infrastructure [2].

In a publication by Wolfowicz et Al. [3], individual vanadium defects were investigated and it was found that the inhomogeneous broadening full width at half maximum (FWHM) measured to be around 750 MHz significantly disagreed with the lifetime limited linewidth reported to be 5 MHz. This naturally leads one to asking why this is the case. One possibility amongst other reasons provided for this disparity is the phenomena of spectral diffusion over short time scales.

SiC comes in different crystal configurations called polytypes which differ in the bonding between individual layers of the material. This thesis attempts to characterize the effects of spectral diffusion within a vanadium doped 4H-SiC polytype as the results could provide greater insight into the role spectral diffusion plays in research involving these defects. This would in turn contribute to the research around its telecom emission wavelengths and hence help in the development of quantum technologies that are compatible with current communication structures. In order to better understand this phenomena, a model was developed to simulate the spectral diffusion occurring within each defect in a sample and an experiment was carried out in the lab to investigate this

further. After acquiring the necessary theoretical basis in the following chapter, the experimental procedures will be covered and model explained together with its result before presenting and discussing the experimental results. Finally, conclusions will be drawn together with suggestions for improvements and possible further research.

Chapter 2

Theory

2.1 Vanadium doping in SiC

Vanadium defects in silicon carbide are introduced into the material by taking the place of a silicon atom within the crystal structure. A picture of the structure of this crystal lattice can be seen in Fig. 2.1a. As previously mentioned, SiC comes in different crystal configurations called polytypes which differ in the bonding between individual layers of the material. By changing how the material is layered, the crystal symmetry and number of inequivalent sites also changes. The structure of two polytypes of SiC, 4H-SiC and 6H-SiC, and the resulting inequivalent sites for each can be seen in Fig. 2.1b. The research laid out in this report revolves around 4H-SiC. Due to the shape of the 4H-SiC silicon carbide lattice, the vanadium defect can introduce itself into two inequivalent sites. Each site comes with a different crystal symmetry and affects the splitting of the energy levels of that defect, these are referred to as the h and k sites and produce distinct absorption lines at different wavelengths.

It is now necessary to lay down some more theoretical ground-work in order to better understand the physical phenomena at play. The propagation of light through various mediums has been researched in great detail, and it is useful to begin with the classical theory of optical propagation, in which the light is treated as electromagnetic waves and the atoms or molecules are modelled as classical dipole oscillators.

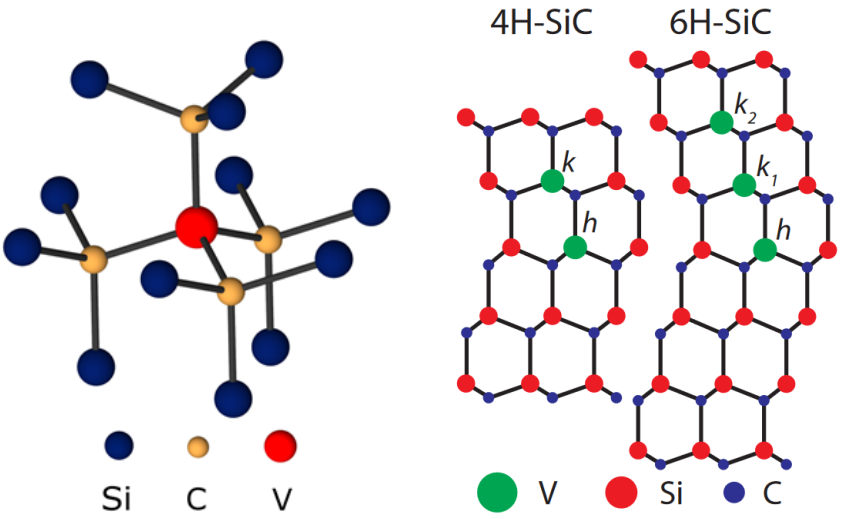

(a) Crystal structure of vanadium doped SiC

(b) h and k sites illustration modified from [3]

Figure 2.1: Vanadium doped 4H-SiC illustrations

2.2 Classical atomic dipoles

In an insulator or semiconductor, the most important contribution at optical frequencies comes from the oscillations of bound electrons within the atoms [4]. These can be referred to as atomic oscillators. The following explanation of the classical theory follows from [4]. The oscillator model of the atom states that each negatively charged electron and the positively charged nucleus form their own electric dipole whose magnitudes are proportional to the separation of each electron from the nucleus. Each individual electron is kept in a stable orbit around the nucleus and can be pictured as being connected to the nucleus by a spring that represents the restoring force for small displacements of the electron from it's equilibrium position. Each dipole has its own resonant frequency ω_{eg}, the frequency required to excite electron from ground (g) to excited state (e), that is determined by the reduced mass of the electron and nucleus system. When light with a certain frequency ω is incident on the atom, it drives oscillations at this frequency. If ω coincides with one of these natural dipole frequencies, the atom can absorb this energy which causes large oscillations of the dipole. Incident light whose frequency is not equal to a resonance frequency will drive atomic oscillations at frequency ω that will introduce a phase lag caused by damping. This explains the slowing down of light as it passes through a medium with a higher refractive index. The absorption spectrum of such a driving process is shown in Fig. 2.2b and is represented by a narrow Lorentzian lineshape.

In the modern day it is understood from quantum theory that what is really occurring is that light absorbed at specific resonance frequencies is causing the electron to jump up to an excited state. The electron can then return to lower energy levels through re-emission of electromagnetic waves.

(a) Visual representation of classical model taken from [4] where the dipoles between the central nucleus and surrounding electrons are represented by springs

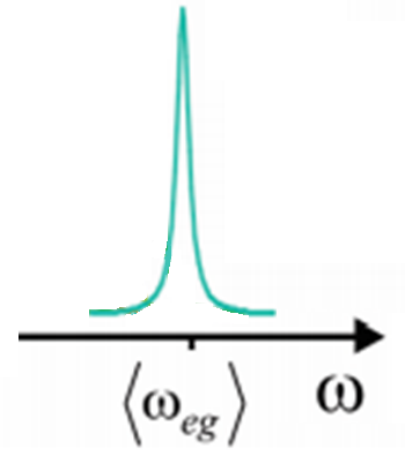

(b) Absorption Lineshape of each Dipole with excitation frequency ω_{eg} modified from [5]

Figure 2.2: Classical description of atomic oscillators

This being said, for simple cases such as the one treated in this paper, the classical model described here is a good approximation of what is actually occurring.

2.3 Hyperfine states and laser absorption

There are multiple interactions which cause the splitting of the vanadium atom's energy levels. Firstly, the crystal field potential causes an initial splitting of the 5 3d orbital states into 2 doublets and 1 singlet [2, 6]. Subsequently, the effects of the spin-orbit coupling between the electron's spin and orbital angular momentum further split these levels into 5 doubly degenerate levels called Kramers doublets [6]. Finally, hyperfine splitting caused by the electron's interaction with the nuclear spin leads to the splitting of these Kramers doublets into non-degenerate energy levels [6]. Due to the 7/2 nuclear spin of vanadium and the 1/2 spin of the electron, one actually ends up with 16 ground and excited states that can be addressed with a laser. For simplicity, a three level system will be considered as higher orders of transitions would go beyond the scope of this paper. The three level system discussed is composed of two ground states here referred to as $|g\rangle$ and $|s\rangle$ which come from the hyperfine splitting of the lowest Kramer doublet and an excited state $|e\rangle$ which arises from the hyperfine splitting of the third lowest energy doublet.

As a result of this splitting, when a laser that is able to excite the electron from the lower energy ground state $|g\rangle$ into an excited state $|e\rangle$ is incident on the material, there is a probability of it first decaying into the other ground state $|s\rangle$ before finally returning to the lowest energy level $|g\rangle$ (see

Fig. 2.3). Experiments dealing with these two ground states and an excited state in any context refer to this configuration as a 'lambda' configuration.

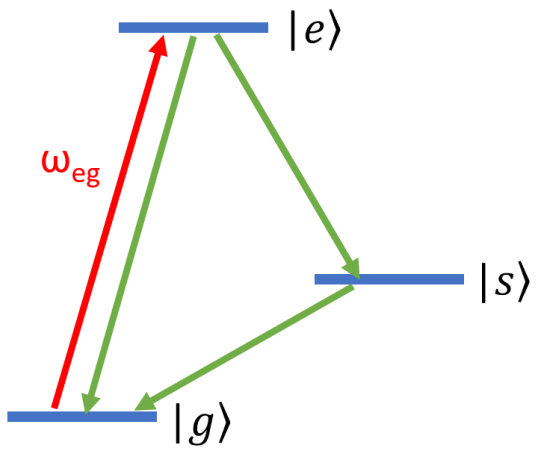

Figure 2.3: Lambda configuration addressed in this experiment. Red: Laser induced excitation Green: Possible decay paths

The relaxation from $|s\rangle$ to $|g\rangle$ takes a certain amount of time which is referred to as the spin lifetime T_1. Measurements of T_1 are quite important for experimentation for quantum memory applications, and if the spectral diffusion of these defects is on a similar timescale to the spin lifetime, then the results of experiments attempting to measure T_1 will be affected by the diffusion. This results from the fact that measuring the rate at which electrons return from $|s\rangle$ to $|g\rangle$ for a particular resonance frequency is done through monitoring of the population of $|g\rangle$. Not only can electrons populate this ground state in vanadium defects through decay from $|s\rangle$, but also through the spectral diffusion of other defects which adds their ground state electron to the population being monitored, therefore making the time measured for ground state re-population reflect multiple processes rather than T_1 only.

The measurement of T_1 is most accurately performed at low temperatures as this reduces the probability of the excited electron dropping straight back down to $|g\rangle$ as illustrated in Fig. 2.3. Low temperatures also reduce the electron phonon coupling, where stronger coupling would make it harder to resolve between the transitions being addressed. For these reasons, the experimental data was collected in the same environment as measurements that aim to measure properties such as T_1 in order for results to be directly applicable to these experiments.

If electrons return first to the higher energy ground state $|s\rangle$, they will remain there for a long enough time to eventually allow a powerful enough laser to remove all electrons from $|g\rangle$. 'Hole burning' refers to the dip observed in the transmission spectrum when performing spectroscopic measurements on the sample. A model developed to simulate the processes mentioned here was created to experiment with varying parameters and is explained in following sections together with more details.

2.4 Crystal perturbations and spectral diffusion

When a crystal lattice is doped with ions, the ions' optical properties are modified by the interactions with the crystal. For weak interactions, the absorption and emission spectra will be discrete lines similarly to how they would appear when isolated in their gas phase, possibly along with a slight shift in their frequency and the splitting of some states [4]. If the interaction is strong, the frequencies of the transitions will significantly differ from those of the isolated ions, and the spectra may be broadened into a continuum [4]. This phenomena will subsequently be treated in more detail using our specific dopant/defect (used interchangeably in this paper as both descriptions are representative) of interest, V^{4+}.

Depending on the placement of the vanadium dopant, it will experience crystal field effects which will cause a shift in its energy levels. The specifics can be calculated using perturbation theory, but this goes beyond the scope of this paper. A more detailed description can be found in [2]. Crystal field effects can be either static or dynamic. The static effects are due to the crystalline symmetry surrounding each dopant and cause the lifting of degeneracy thanks to the effects of the electric field. The consequence of this static effect is an inhomogeneous Gaussian broadening of the absorption lineshape representing the dopants resonance frequencies overall [5]. An illustration of the static effect on the ensemble's overall lineshape can be seen in Fig. 2.4.

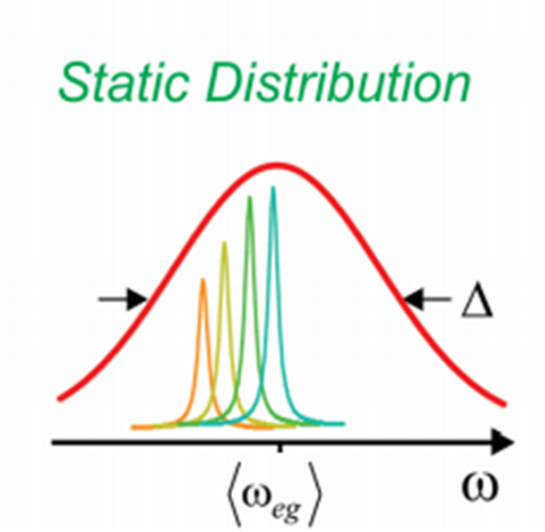

Figure 2.4: Illustration of inhomogeneous broadening of width Δ around resonance frequency $\langle\omega_{eg}\rangle$ taken from [5]

There are also dynamic effects affecting the energy levels which together result in the phenomena of Spectral Diffusion. One of the dynamic effects originates from vibronic coupling in the system. Crystal vibrations displace the atoms from their equilibrium positions, changing the electric field the dopant experiences. This alters the perturbations experienced by the energy levels, ultimately coupling the vibrations to the electronic levels of the defect [4]. Transition metal ions such as V^{4+} are particularly susceptible to the crystal field effect as the outermost electron is found in the 3d shell, which has a large radius and is not shielded by filled outer shells [4].

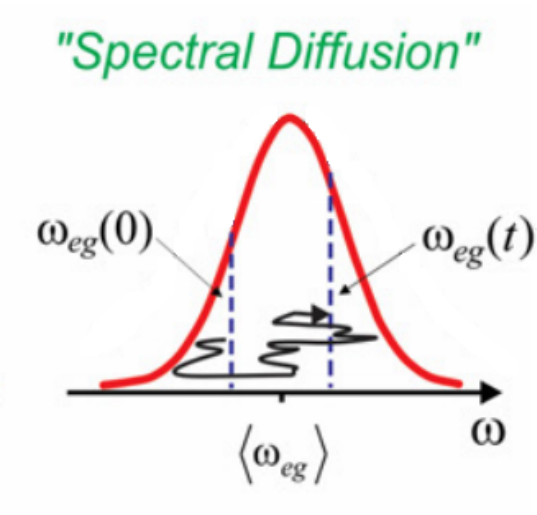

Figure 2.5: Distribution of frequencies the transition within one vanadium atom can take. Once Lorentzian, now Gaussian. Image from [5]

More importantly, the influence of the electric field of an incident laser during experimentation that varies over time will provide a more significant contribution to the dynamic effects experienced by the vanadium defect's energy levels. These dynamic effects cause the excitation frequency between the statically split energy levels to go from being a well defined value represented by a Lorentzian such as the one in Fig. 2.2b to a less clear value that fluctuates over time represented by a Gaussian like the one shown in Fig. 2.5. It is important to note that the spectral diffusion each defect can experience is limited by its environment to those frequencies included in this distribution.

2.5 Random walking to model spectral diffusion

Spectral diffusion can be viewed as the result of random fluctuations of the energy levels within each vanadium defect. In order to statistically describe these time-dependant fluctuations, time-dependant probability distributions are required and hence a stochastic equation of motion. Nitzan [7] shows that starting from a random walk model, where (in the one dimensional case) at any given time the object in question is able to move a certain distance in one of two directions, one is able to reach an equation of motion that can describe such a fluctuating object. This turns out to be the diffusion equation:

$$\frac{\partial f}{\partial t} = D\frac{\partial^2 f}{\partial x^2} \tag{2.1}$$

Where x is the frequency of the transition. Starting from the initial condition $f = P(x, t_0) = \delta(x - x_0)$, the solution to this equation is a conditional probability density which has a Gaussian form:

$$P(x, t; x_0, t_0) = \frac{1}{\sqrt{4\pi D(t - t_0)}} \exp -\frac{(x - x_0)^2}{4D(t - t_0)} \tag{2.2}$$

Where x_0 is the mean frequency value over which fluctuations occur and t_0 is the initial time (0 in this report's case). The width of this probability distribution can be calculated to be $\langle \delta x(t)^2 \rangle = 2Dt$ where $\delta x(t) = x(t) - x_0$. This means that the width of the distributions broadens with time as $\sqrt{2Dt}$ as illustrated in Fig. 2.6.

The model discussed in the following chapter does not use a random walk in which each step has the same size. The step size at each point in time is determined by sampling from a Gaussian representing the broadening of the vanadium defect similar to the distribution shown in Fig. 2.5. Nevertheless, a square root dependence in time is expected for this approach as well [8].

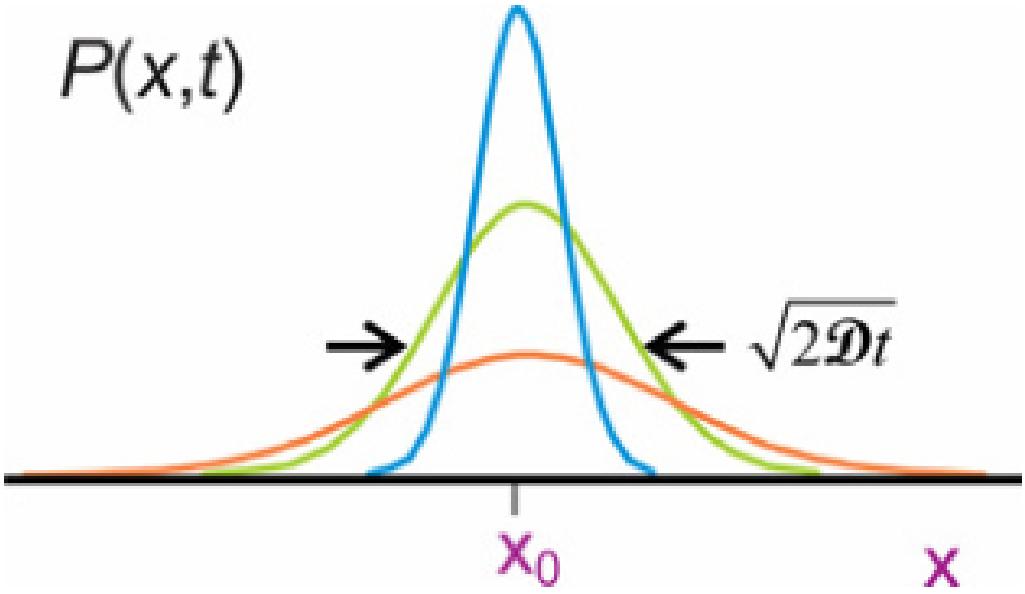

Figure 2.6: Broadening of the distribution over time taken from [5]

2.6 The Spectrum Analyzer and FFTs

One of the most important pieces of equipment used in this experiment is the spectrum analyzer that is able to take a time varying signal and convert it into a frequency spectrum thanks to an algorithm called the 'Fast Fourier Transform' (FFT). Some periodic time-dependant signals can be very difficult to interpret by analyzing them as they appear on a graph due to for example the presence of noise. Thankfully, the Fourier theorem has proven that such signals can be decomposed into a linear combination of sine waves of different frequencies. Each sine function will have a different magnitude, and therefore the sine components that are the largest will appear as sharp peaks on a graph that plots frequency against the magnitude.

The spectrum analyzer used (SR785) digitizes the signal at a high sampling rate and takes advantage of Nyquists's theorem to ensure an accurate representation of the signal. This theorem states that as long as the sampling rate is greater than twice the highest frequency component of the signal, then the sampled data will accurately represent the frequencies of the input signal [9]. The SR785 can sample up to a rate of 262 kHz and therefore is limited to presenting frequency spectra spanning at most 102.4 kHz. This is done through the use of an anti-aliasing filter that restricts the bandwidth to frequencies less than or equal to 102.4 kHz [9].

As a consequence of Nyquist's theorem, the resulting spectra will have half as many bins as the number of points sampled. This presents a problem. A particular frequency might be split into two neighbouring bins rather than be contained in one bin only. So although this computation is quite fast overall, there is the risk of missing the signal frequency of interest. This can however be improved by lengthening the sampling time and changing the span of the spectrum [9].

The graphs presented in the results from measurements using the SR785 display units of dBV_{rms}. The original input signal is in volts, but computing the FFT of this signal results in a list of complex numbers that contain information on the amplitude and phase of the signal. The plots show the magnitude of the signal after undergoing a Fourier transform against the various frequency components calculated using $|V| = \sqrt{x^2 + y^2}$ with x and y being the real and imaginary parts of the FFT. The result is converted to dB and plotted linearly. The data gathered is a result of averaging 200 individual spectra all with the same weight in order to remove noise.

$$\mathrm{dB}V_{rms} = 10log_{10}(|V|)^2 \tag{2.3}$$

Another common presentation of such spectra is in power spectral density (PSD) units. The conversion between the units used here and PSD units is relatively simple. The input voltage the signal analyzer receives needs to be divided by the square root of the bandwidth Δf of frequency for each bin. The FFT spectrum assumes that the signal inputted is periodic, which is not always the case. In order to avoid unnecessary noise in the spectrum, the signal analyzer multiplies the signal by a function that is periodic as well as continuous and smooth at 0. This is referred to as 'windowing'. An extra correction factor is included in the SR785's PSD units calculation due to the windowing involved which was found to be roughly a factor of 1.4.

$$\text{PSD (decibel units)} = 10log_{10}(\frac{|V|}{\sqrt{\Delta f} \cdot 1.4})^2 \tag{2.4}$$

2.7 Noise sources

Unwanted noise must always be considered when performing measurements of a particular signal. Therefore, the possible noise sources should be recognized in order to understand how to best design each new experiment to minimize the background's interference with your signal of interest. Noise stems from multiple sources which will now be covered in some more detail.

One source of noise referred to as the 'Shot noise' arises from the discrete nature of the charge carriers [9], in this case electrons. There is always some small degree of non-uniformity in the electron flow, and this generates noise in the current which is reflected as voltage noise when the current passes through a resistor. However due to the small charge of an electron, this noise source is not

of much concern in this particular experiment.

A few other sources of noise arise from the resistors in the setup. One such a source is 'Johnson noise', which arises due to the thermal fluctuations in the electron density within each resistor [9]. Another source which will be found to be quite noticeable is the '1/f' noise, which turns up on the spectrum as a large jump in magnitude of the signal at low frequencies. This 1/f noise is either due to the resistors present within the signal analyzer or from the SiC itself [9, 10]. Every resistor found within photodiode and spectrum analyzer will contribute to these forms of noise.

Noise can also occur due to the interaction of different setup components with each other. This can occur through a process known as capacitive coupling. An AC voltage from a nearby piece of equipment can couple to another signal through a stray capacitance. An example of this is the possible coupling of the power supply of the spectrum analyzer to the circuit component responsible for carrying the input signal. Even if this capacitance is low, there is the potential for the noise to be strong enough to overwhelm a weak signal [9]. All sources mentioned have been kept in consideration during experimentation.

Chapter 3

Experimental methods and setup

3.1 Experimental setup

The setup of the experiment is as follows. (After being redirected with the required optical components,) a diode laser with variable wavelength is directed onto the sample found within a cryostat. The cryostat consists of multiple layers: a vacuum cavity for insulation from the outside temperatures, liquid nitrogen chambers for initial cooling, a liquid helium chamber for further cooling, and finally the sample space which is also cooled with liquid helium. This allows for measurements to be made at temperatures down to 2K. After impinging on the sample, a percentage of the laser light is absorbed depending on the number of defects which are currently in resonance with its frequency. The light that is not absorbed is coupled into a multimode optical fiber which is connected to a photodiode and the resulting transmitted signal is sent to the signal analyzer where an FFT is computed and displayed.

In order to understand the effects of the sample on light passing through it, the measured signal will need to be compared to a reference signal. This was acquired by setting up flip mirrors before and after the cryostat together with another 2 fixed mirrors which allowed for the redirection of the laser light around the sample, but still allowed it to couple into the photodiode. After the light passes through and interacts with the sample, the resulting laser power is significantly reduced as it reaches the photodiode. In order to allow for a direct comparison of the signals, the same signal power needs to arrive to the signal analyzer from the photodiode both after it is transmitted through the sample and when it is directed around it. After fixing a certain power of the signal received after the laser passes through the sample, the same power was fixed for the 'bypass' route through the use of a neutral density filter. A light dump was included in order to absorb the light reflected by the neutral density filter. A diagram of the described setup is displayed in Fig. 3.1.

It is important to note that the laser diameter is around 100 micrometer, much smaller than the sample size. Therefore, only the defects through which the laser passes have a chance to become

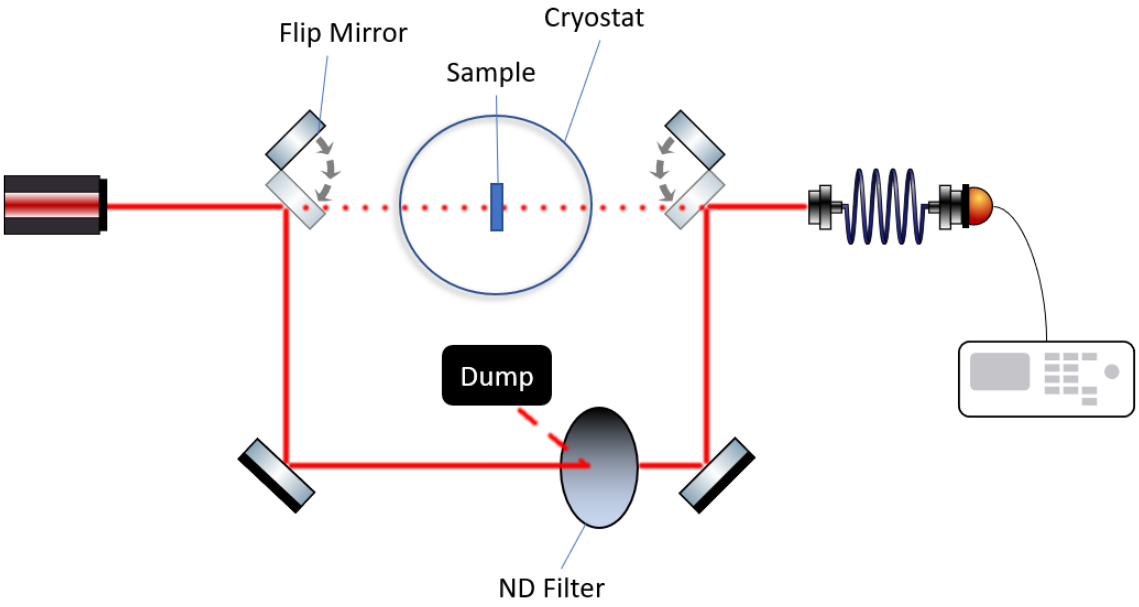

Figure 3.1: Diagram of the setup

excited. The structure of the sample is assumed to be homogeneous, which allows any results to reflect behaviour of the sample as a whole.

3.2 Background noise characterization (measurements)

Due to the low signal expected from the effects of spectral diffusion, it was necessary to first investigate the noise floor behaviour of the setup. This was done through the recording of Fourier transforms for the signals generated by the signal analyzer and subsequently those resulting from the addition of more components such as the photodiode and the laser light itself. A comparison of the noise floor evolution can be observed in Fig. 3.2. Although there is noise associated with the photodiode when it is off, turning it on removes this and the laser signal is clearly noticeable within the spectra. This matches with initial expectations given that the noise floor of the signal analyzer as mentioned in its user manual [9] is easily overwhelmed by the laser signal passing through the photodiode. All measurements were completed by making sure the same power was transmitted by the photodiode in order to allow for a direct comparison of the signals.

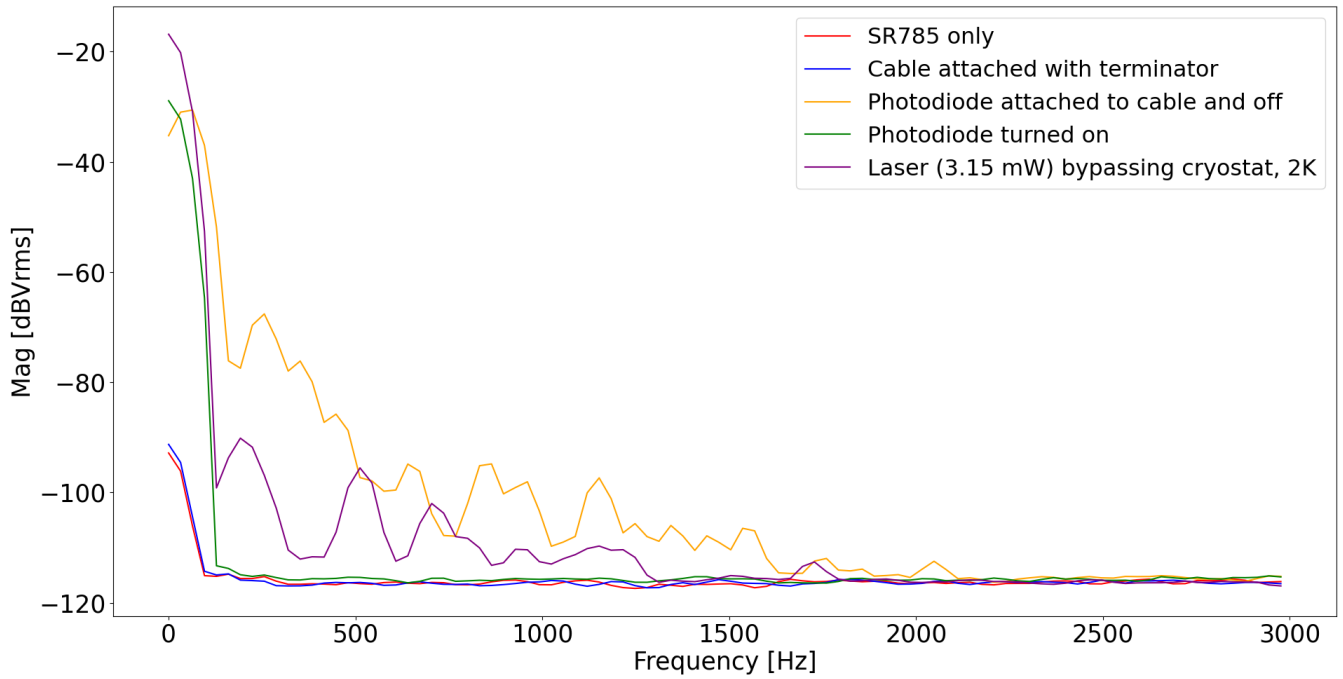

Figure 3.2: Comparison of spectra as components are added

3.3 Computer Model

A model was developed in python to attempt to simulate the behaviour of the spectrally diffusing defects throughout the entire sample. This was achieved through the manual generation of the inhomogeneous distribution of the defects as a Gaussian with a typical full width at half maximum (FWHM) of 30GHz. More specifically, every defect's initial resonance frequency (which varies over the spectrum due to the static crystal field effect) is represented as a difference or 'detuning' from the incident laser's frequency.

The horizontal axes of the distributions in the model mark the difference between the frequency of the laser and the resonance frequency of a certain amount of defects. This is referred to as the 'detuning'. The distribution is centered around a mean associated with the frequency for which most defects are in resonance with the laser and hence have 0 Hz detuning. This difference plotted on the x axis is ordered into bins representing a range of such frequencies. If 30 defects had an initial detuning between 3 and 3.1 GHz, then the point (3.05, 30) might be included in this Gaussian (depending on how many bins are used). The sum of the number of defects in each bin on this Gaussian plot should give the total number of defects in the entire sample. The total number of defects addressed in the simulations was not representative of the full amount found inside the sample used experimentally. It needed to be scaled down due to computational limits.

At each time step, the number of defects represented in each bin is shifted by applying a Gaussian

locally to each point within every bin with a varying FWHM. This is the diffusion width which reflects the spectral diffusion's diffusion speed. If a defect's detuning were to take a value lying outside of the outermost bin and therefore out of the plot, it will instead cycle into the bin on the other end of the distribution. This boundary condition allows for a rough representation of defects diffusing in and out of the main distribution of concern. The modeled approach is a Markovian process, where each defect's transition frequency in the following step is solely determined based on the current frequency and not from any of it's past frequencies. This gives each defect's energy level the possibility to diffuse as far above or below the sample's mean resonance frequency as they like. In reality, the energy levels are not able to diffuse this much due to restrictions imposed by the vanadium atom. The approach taken was a necessary simplification of reality also in order to accommodate the limits imposed by the computational power available.

After such a procedure, the bins containing the shifted number of defects are saved for the following time step, and the bins which make up the central 10 MHz are saved separately as well. These central bins roughly consist of the defects that would get excited by the laser at this point in time. The 10 MHz value reflects the minimum (lifetime limited) width of a defect's absorption spectrum of 5MHz. Only those defects with resonance frequency sufficiently close to the mean would be able to absorb light.

If the hole burning effects are to be observed, then another component is introduced into the code which targets those central bins that would feel the laser. A binomial distribution is applied to each point within these central bins, with a certain probability of being excited into $|e\rangle$ and relaxing into $|s\rangle$. If this occurs, it will be removed from the distribution and saved in a separate array. These points will have the opportunity to return through another binomial distribution with a lower chance of success based on T_1 in the following time steps, which reflects the relaxation process.

Chapter 4

Results and Discussion

4.1 Model Results

A plot of the evolution of the defect resonance frequency distribution is presented in Fig. 4.1 and 4.2. Figure 4.1 shows curve fits made of an initial delta function condition as given in the theory, where all defects were in resonance with the laser's frequency to begin with. Figure 4.2 does the same but for a more representative defect spread where the starting point is a Guassian distribution with a FWHM of 30 GHz. The fitted function used is shown below:

$$\text{FWHM} = \sqrt{2D(t - t_i)} \tag{4.1}$$

Where D represents a diffusion constant. The delta function itself was omitted to improve legibility. The square root fit provided needed to be offset by a certain amount t_i in Fig. 4.2b since the initial condition for the model was not a delta function as the theory started with, but an already partially widened distribution. The offset value t_i for Fig. 4.1 is set to 0.

The times chosen for Fig. 4.2 are simply a consequence of storing alternating distributions rather than all of them to save computational time. The number of defects used in these simulations are not representative of the amount found in an actual sample which in total is around 10^9, but the plots illustrate the flattening just as clearly. The range of detuning is also not always reflecting the actual case, but this has no impact on the qualitative behaviour observed. It is immediately seen that the plots are in clear agreement with the theoretical result obtained from the diffusion equation. Plotting the width against the time increments yields a plot that can be fitted with a square root function as shown in Fig. 4.1b and 4.2b. It is important to note that the time unit is arbitrary in this model since the rate of diffusion for this process is unknown, and therefore the individual values of the diffusion coefficients found from the fit don't hold any weight on their own. This being said, an interesting continuation of this component of the model would be to investigate the relationship between the diffusion constants found from the fit and the widths of the spectral diffusion distributions used to generate the data.

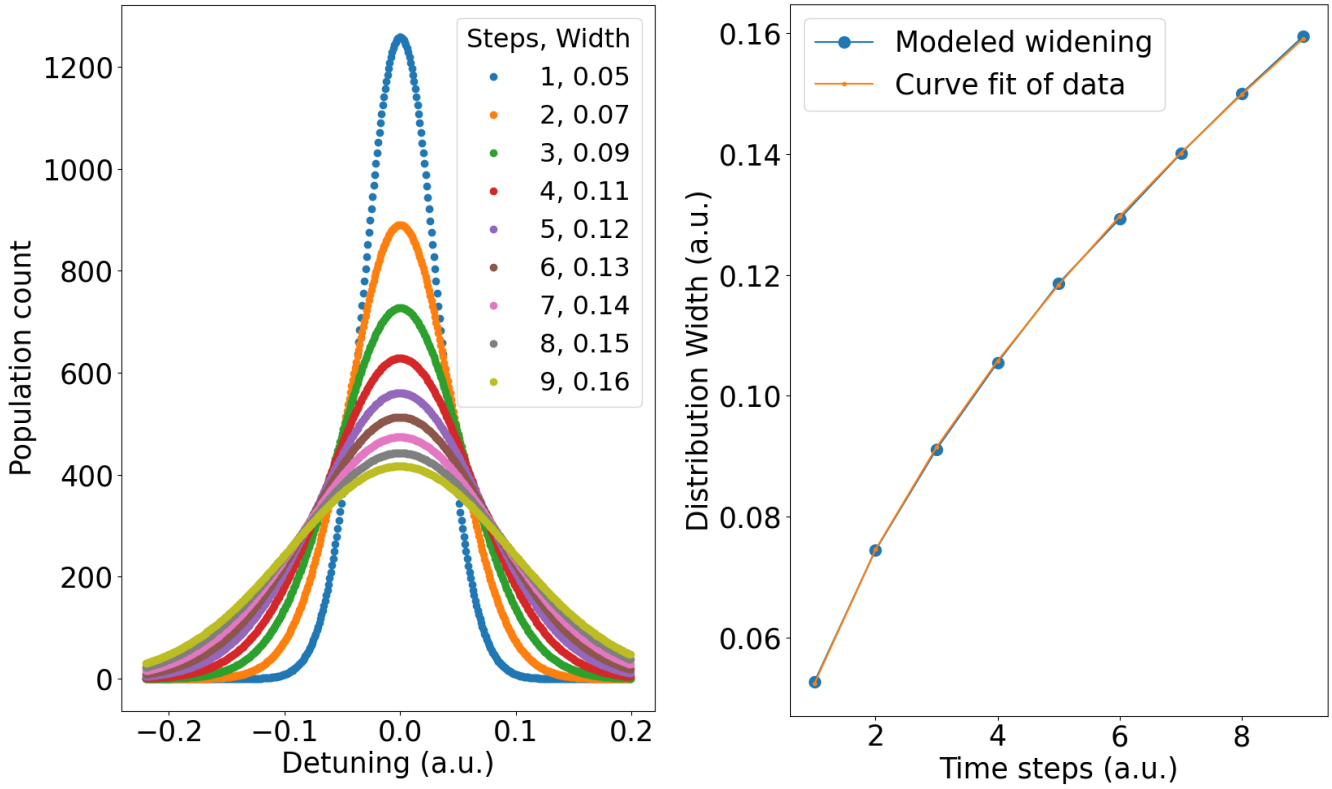

(a) Probability distribution flattening

(b) Distribution width over time

Figure 4.1: Modeled evolution of defect detuning probability distribution over time starting from a delta function

The number of defects in the central bins saved at each time step can be converted into a frequency spectrum by computing the Fourier transform of the saved data. The width of the sampling distribution, which is related to the speed of spectral diffusion, was varied over multiple simulations and the corresponding spectra were compared to find some characteristic difference related to the change in width of this distribution. The Fourier transforms of two simulation runs can be found in Fig. 4.3. From this figure it can be concluded that for the timescales over which these simulations were run, it is not possible to find any net differences in the spectra.

The hole burning effects when included in the simulation can be immediately spotted at any time step other than t_0 by noticing the central bin as shown for example in Fig. 4.4 having a significantly lower number of defects compared to the rest of the distribution. The parameters that control the rate of electrons decaying from $|s\rangle$ into the ground state $|g\rangle$ can be varied, but this again did not seem to influence the spectra obtained from the FFTs under the time scales investigated.

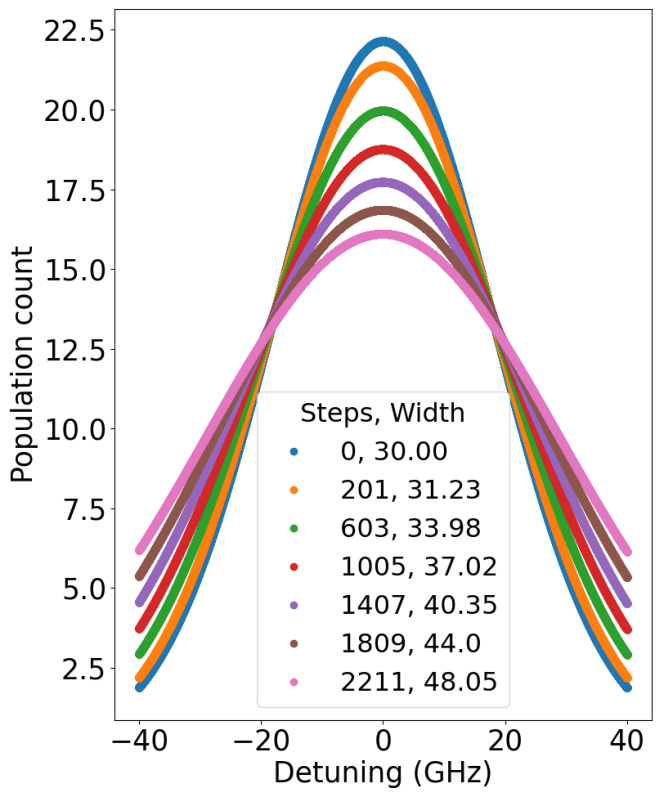

(a) Probability distribution flattening

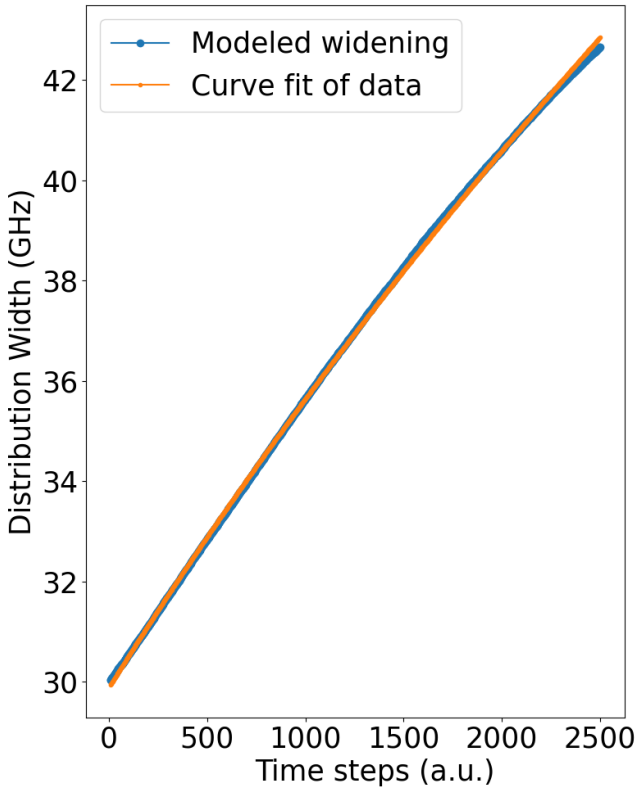

(b) Distribution width over time

Figure 4.2: Modeled evolution of defect detuning probability distribution over time starting from a 30 GHz distribution width

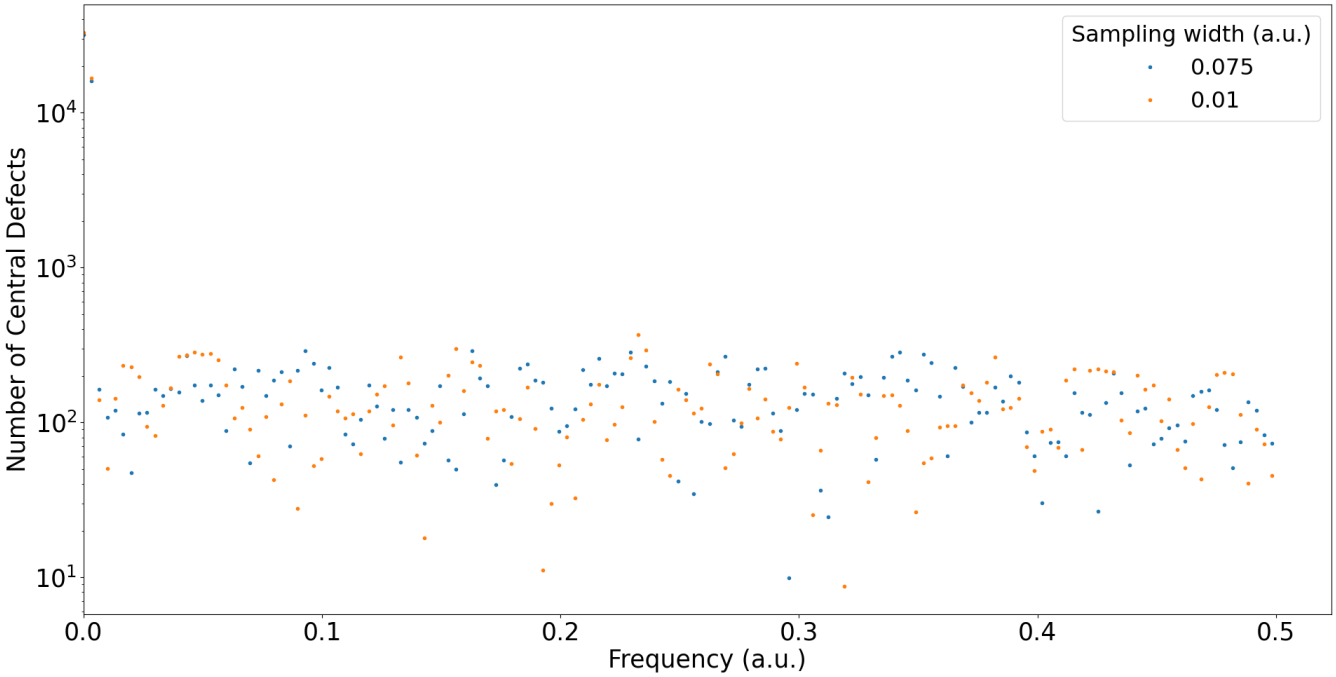

Figure 4.3: Frequency spectra of variations in central defects for different spectral diffusion sampling widths

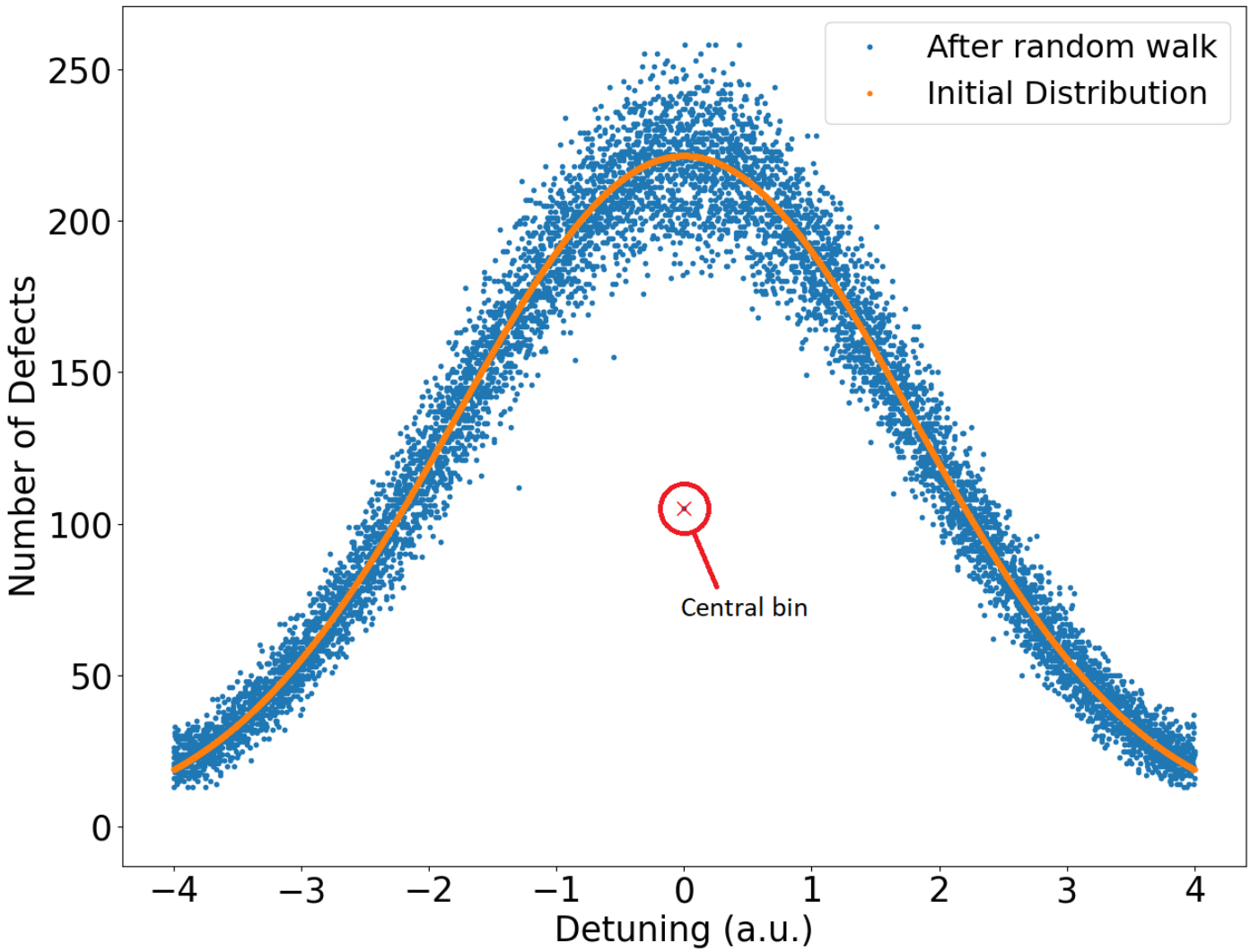

Figure 4.4: Hole burned in spectrum's central bin. Notice the net population difference between it and neighbouring bins that occurs as a result of some of those defects absorbing the light and remaining in $|s\rangle$ for some time.

4.2 Experimental Results

Measurements were attempted for different gain settings on the photodiode, but it was concluded that no gain (0 dB) was the most effective for the purpose of these measurements as it allowed for the noise floor to remain relatively low with respect to the signal. The frequency spectrum of the signal received after the laser passed through the sample was compared against the signal when it bypassed the sample using the mirror setup and is shown in Fig. 4.5. There does not appear to be much difference between the two spectra other than the difference in noise after 2 kHz which will be addressed shortly. This indicates that any peaks observed are most likely not due to the laser's interaction with the vanadium defects. This means that these frequencies are likely related to some laser effects or external laboratory factors such as vibrations of the setup components potentially caused by the cooling apparatus used for the cryostat. Mechanical oscillations as well as laser fluctuations could be reflected in the signal through particular peaks. Although these spectra are only for the data gathered for a 0.6V signal, the other spectra display the same similarity and can be found in appendix A.

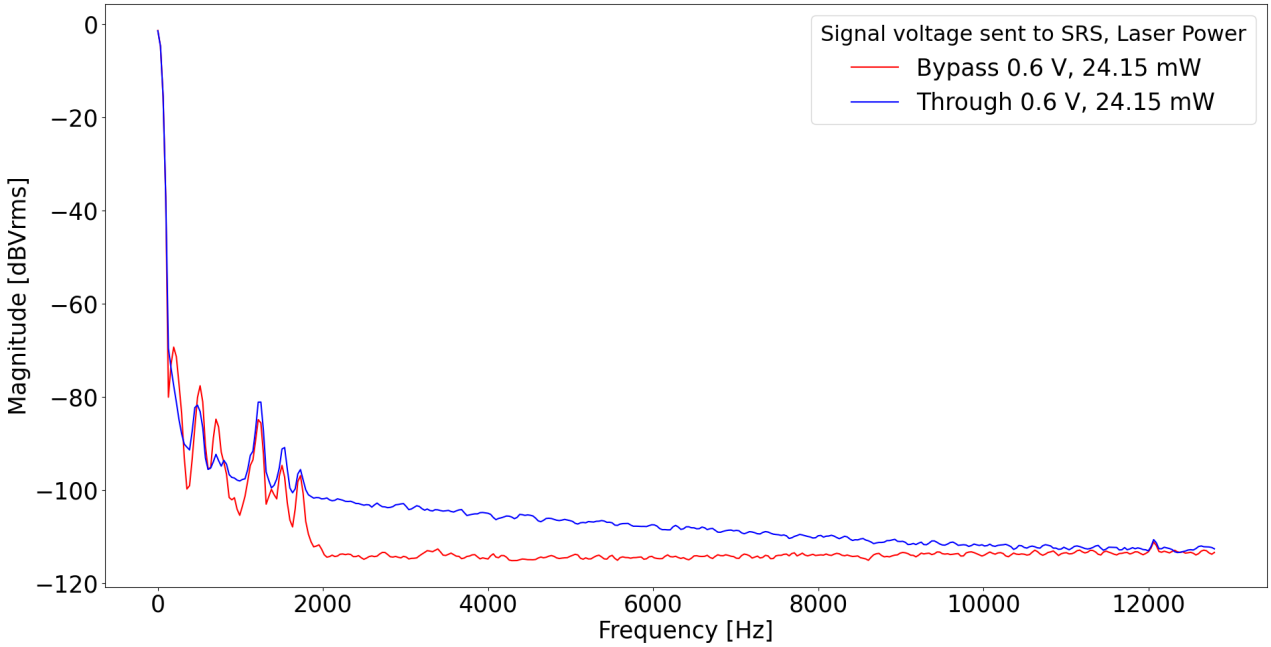

Figure 4.5: Signal spectrum for light (1278.76 nm) passing through as well as bypassing the sample at 2K

The difference between the frequency spectrum of the transmitted signal through the sample and the signal of the bypassing laser for all laser powers at temperatures of 2 Kelvin and room temperature were calculated and plotted in Fig. 4.6 and 4.7. A qualitative comparison shows that at 2 Kelvin, there appears to be a significant difference between the signal received after passing through the sample as opposed to bypassing it. This arises from a significantly elevated noise

floor after around 2 kHz frequencies for the laser passing through the cryostat. In contrast, the difference seems to have completely disappeared when measuring again at room temperature. It is important to consider that some optics were realigned between these measurements at different temperatures, but this should not have greatly affected the overall shape of the graphs observed. This shows that something inside the cryostat is responsible for the addition of significant noise at lower temperatures and hence it can be concluded at the very least that cooling down the sample and its surrounding environment to lower temperatures has a noticeable impact on the signal recorded. It is difficult to associate this temperature dependence with the vanadium defects, since the difference observed in Fig. 4.6 is also present in Fig. 4.7a which relates to a laser completely off resonance with all defects in the SiC sample. Were this difference to be due to the vanadium, the shape of the spectra should have changed in some way depending on how much on resonance the laser frequency is. By integrating the area under each curve and plotting these values against the respective powers, there is a linear increase as one might intuitively expect from the relationship between power and intensity. The plot used to observe this trend can be found in Appendix 5.5.

One more difference to consider is the difference between the spectra of the light passing through the cryostat near the 0 detuning wavelength and completely off resonance as shown in Fig. 4.8 and 4.9. A couple features stand out in Fig. 4.8 when analyzing the higher laser powers, namely the peaks around 1230 nm and 1500nm. Although there is still a small bump around 1230 nm off resonance in Fig. 4.9, the magnitude of the signal is significantly reduced compared to Fig. 4.8. The peak at 1500 nm is completely absent for the off resonance wavelength. This is an indicator that something inside the cryostat is being addressed when a laser of wavelength closer to the resonance frequency of most defects is incident on the sample. As previously noted, since the peaks are all also present in the respective bypassing signal spectra and the difference in noise observed is found both on and off resonance, this difference in the spectra is also unlikely to be defect related and perhaps related to the laser itself.

Despite the interesting observations that can be made from the results presented in this paper, it is difficult to conclude on what exactly the cause of these differences might be. It is clear that there is some interaction occurring inside the cryostat that is certainly temperature dependant as can be seen from comparing Fig. 4.6 and 4.7b and possibly also dependant on the wavelength of the laser used, but it cannot be concluded that these interactions are related to the vanadium defects present within the sample due to the great similarity of the peaks observed in the signals that bypass and go through the sample as well as the noise floor difference found on and off resonance with the defects.

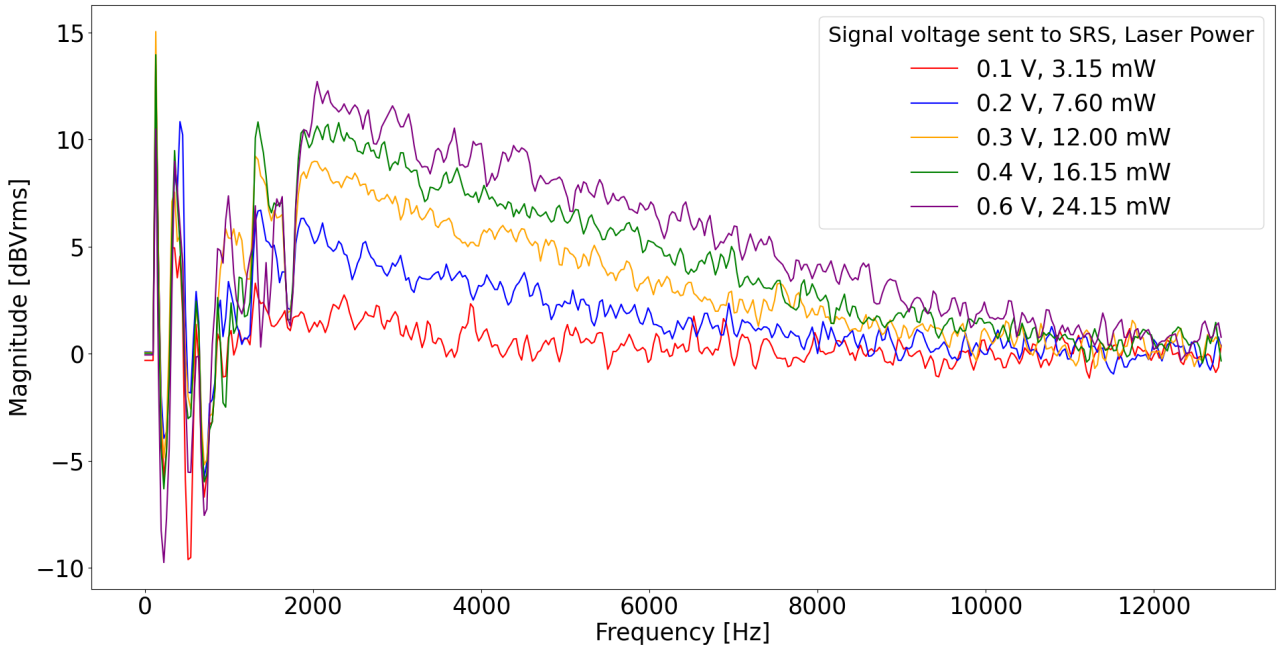

Figure 4.6: Differences between signal spectra for light at 2 Kelvin on resonance with vanadium defects passing through the sample, 0dB Gain

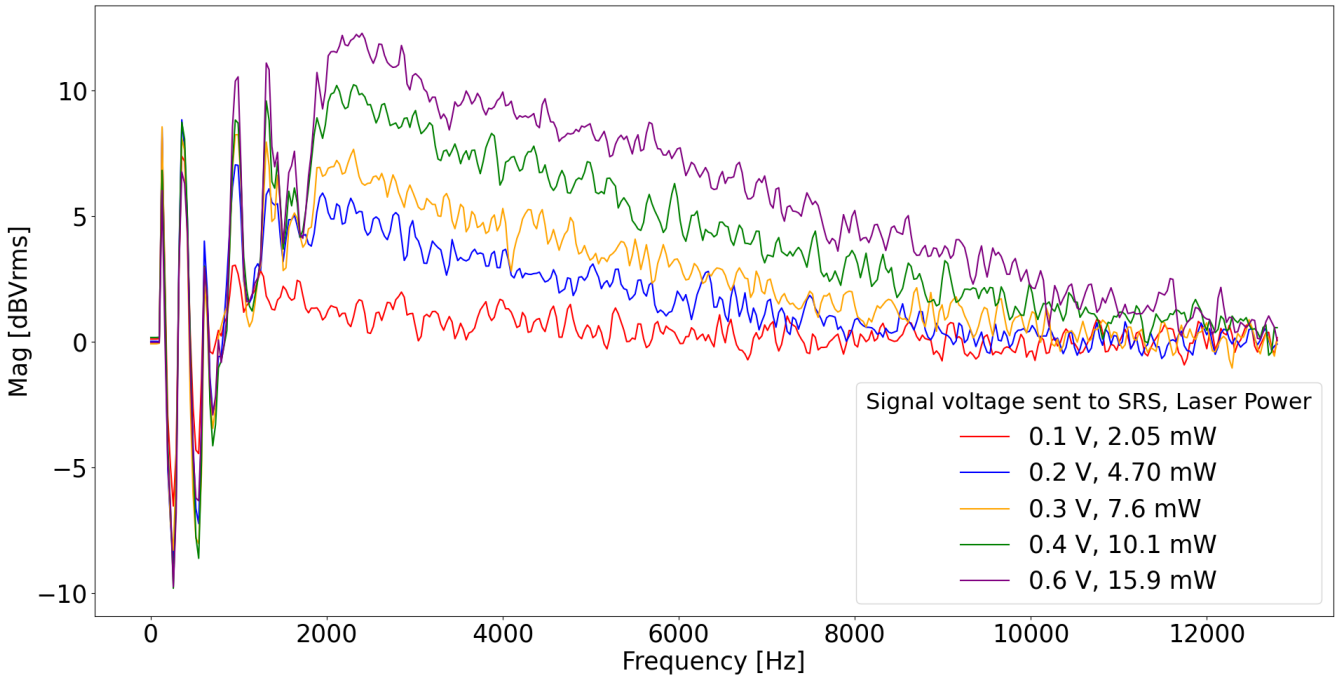

(a) 2 Kelvin, 1280.00 nm

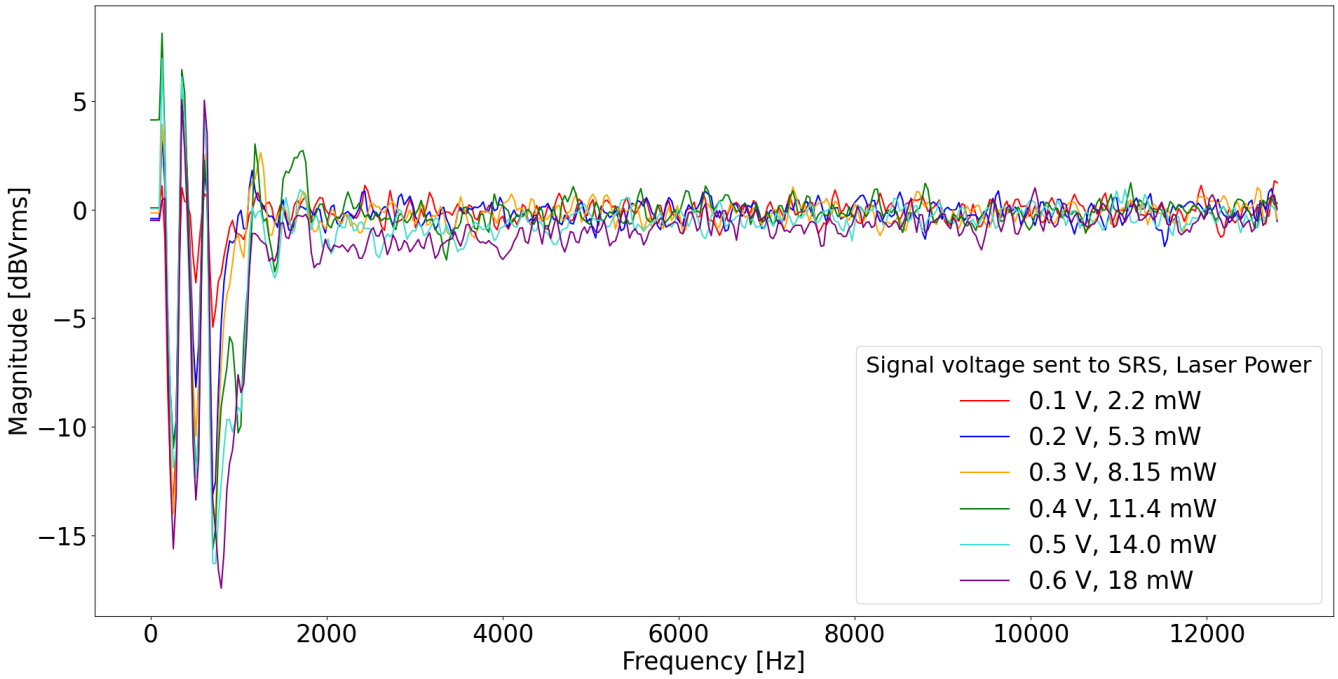

(b) Room Temperature (300 Kelvin), 1278.76 nm

Figure 4.7: Differences between signal spectra for light at 2 Kelvin and room temperature passing through the sample, 0dB Gain

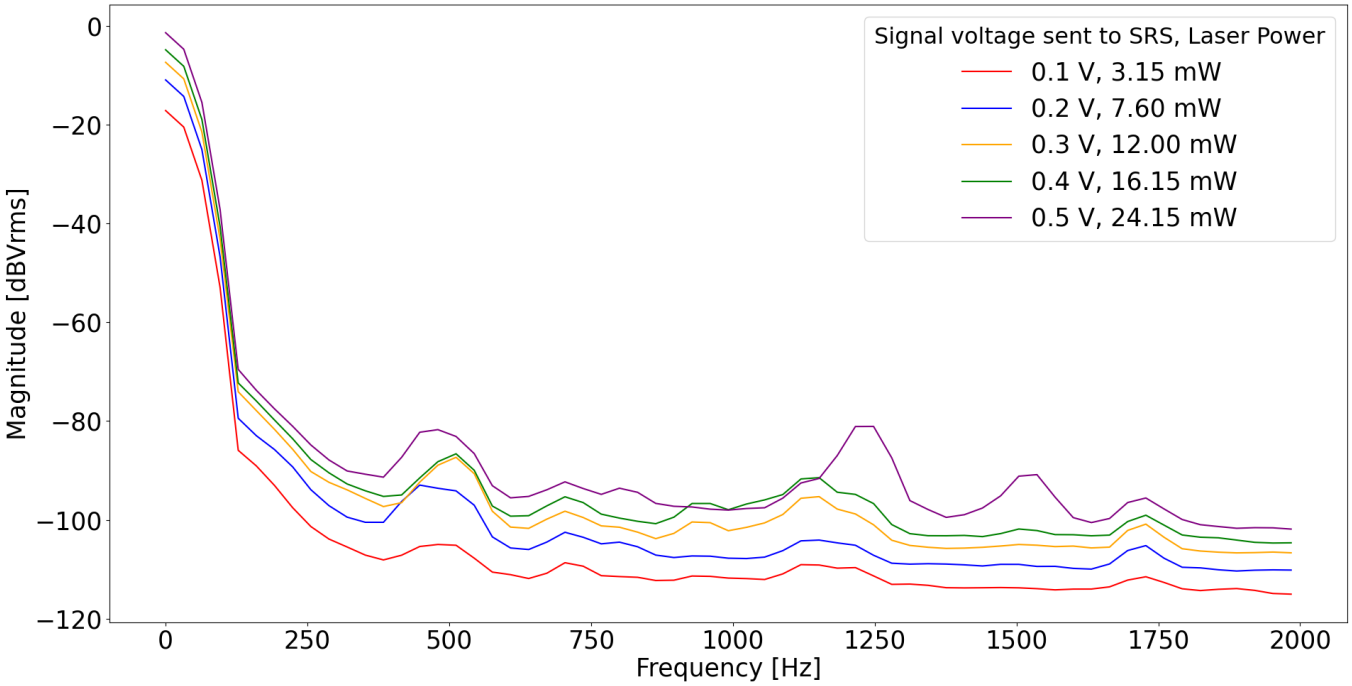

Figure 4.8: Signal spectrum for light (1278.76 nm) passing through the sample at 2K

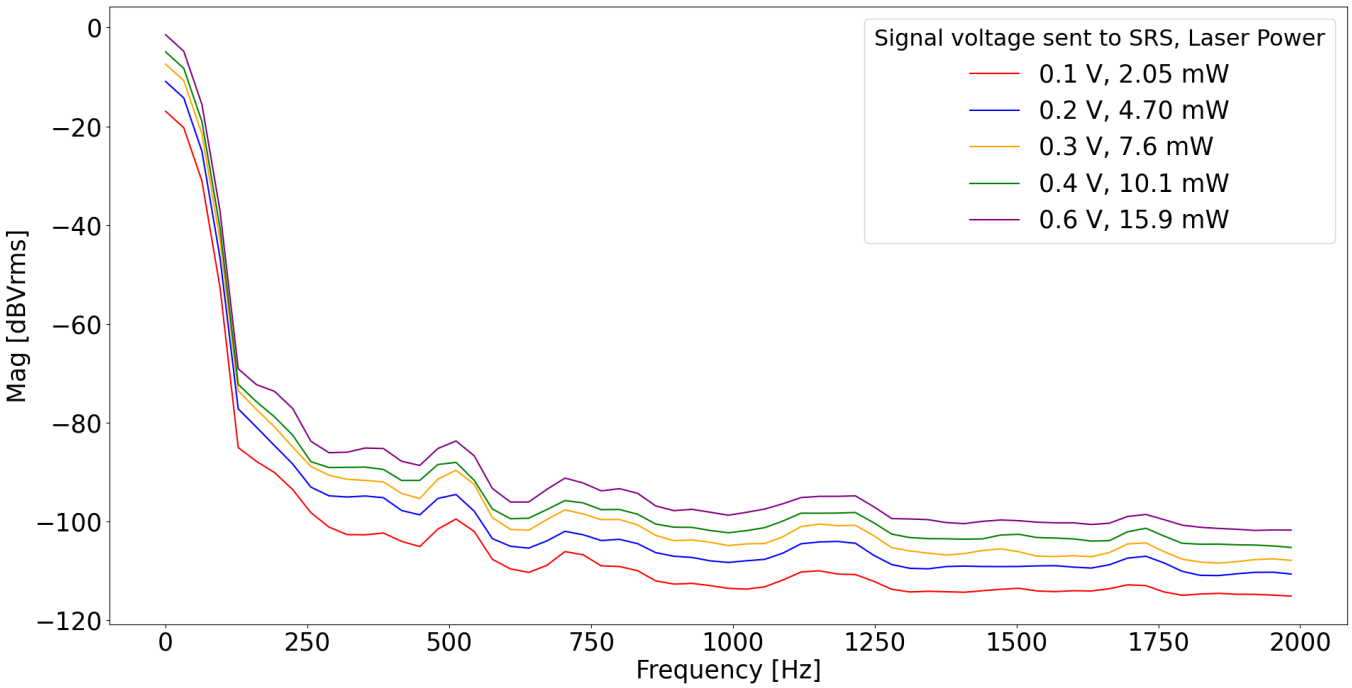

Figure 4.9: Signal spectrum for light (1280.00 nm) passing through the sample at 2K

Chapter 5

Conclusion

This paper attempted to uncover more information on the phenomena of spectral diffusion occurring within a 4H-SiC sample containing V^{4+} defects in order to provide greater insight into the role spectral diffusion plays in influencing research involving these defects. A model was developed in python which was found to be in great agreement with the theory of diffusion, where the flattening of the probability distribution describing the spectrally diffusing energy levels of each defect within the sample was found to be proportional to the square root of the time passed. One extension of this model would be to investigate the relationship between the width of the spectral diffusion distribution for each defect and the diffusion constant describing the widening of the inhomogeneous distribution associated with the doped sample as a whole. FFTs of the time varying central frequency population in the sample were computed and compared for different spectral diffusion sampling widths, but no differences were found over the time scales used. It should be considered that the energy levels within each vanadium defect should not be free to diffuse as far above or below the mean resonance as they like in the real life case. This was not accounted for in this model and would have an impact on the outcome and the specific mathematical boundary conditions and descriptions required to properly simulate this environment. Therefore, an improvement to be made to the model would be to include this condition and observe the change in behaviour of the system.

In parallel with the modelling, an experiment was carried out where comparisons were made between signals arising from the laser light on its own and the signal resulting from the light passing through a V^{4+} doped SiC sample situated within a cryostat. Although no different peaks were found comparing these two kinds of signals, a clear heightening of the noise floor was observed when the laser passed through the sample at 2K. This difference vanished when the experiment was repeated at room temperature, which indicates some temperature dependant effect occurring within the cryostat. Furthermore, comparing signals of lasers off and on resonance with the defects in the sample showed a change in the intensity of the peaks found around 1250 and 1750 Hz and even the appearance of a new peak at 1500 Hz. The peaks of these signals when compared to their respective bypassing laser signal as well as the noise floor difference comparing on and off resonance

laser frequencies are not much different. This implies that these peak differences are not due to the defects, but potentially simply due to the effects form the laser itself. These insights should be explored and expanded on further in future research in order to obtain a better understanding of spectral diffusion in vanadium doped SiC.

Appendix A: Other differences between bypass and through sample signals

Below are additional plots where the frequency spectrum of the transmitted signal after the laser passed through the sample was plotted against the spectrum of the signal for the laser bypassing the sample. This was plotted separately for different laser powers and corresponding photodiode signal voltages.

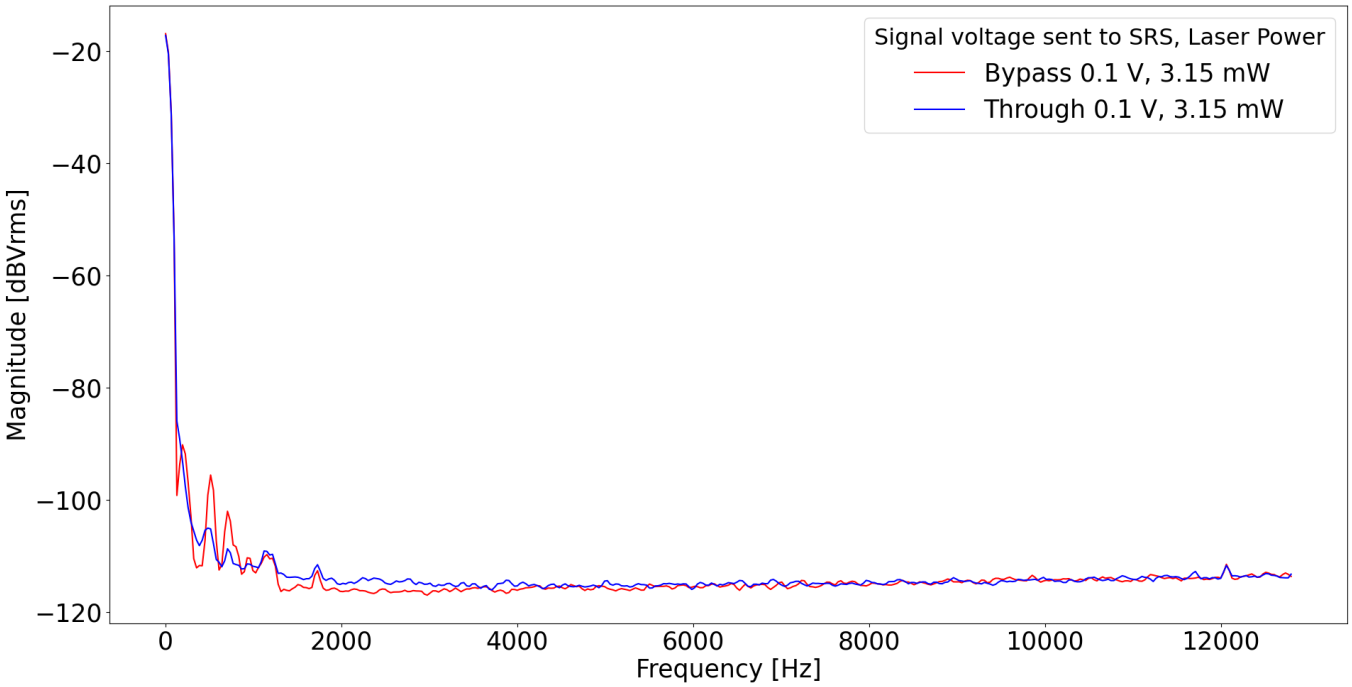

Figure 5.1: Signal spectrum for light (1278.76 nm) passing through as well as bypassing the sample at 2K

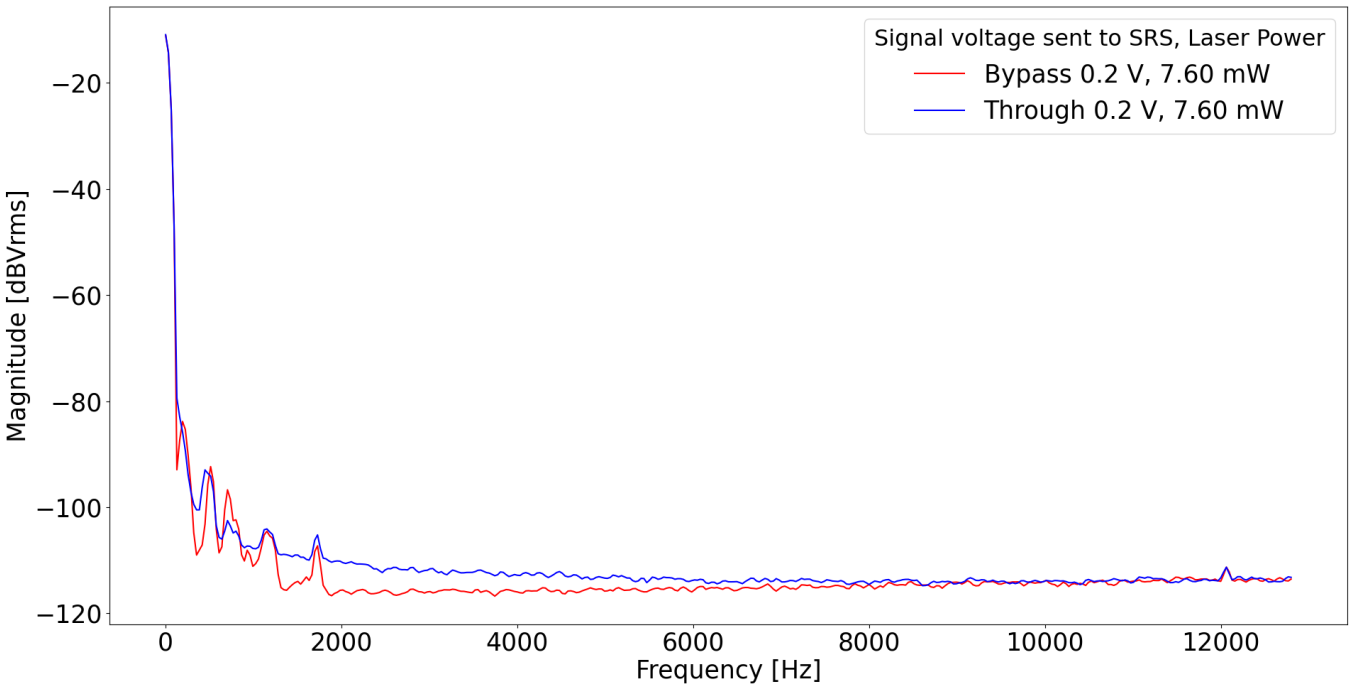

Figure 5.2: Signal spectrum for light (1278.76 nm) passing through as well as bypassing the sample at 2K

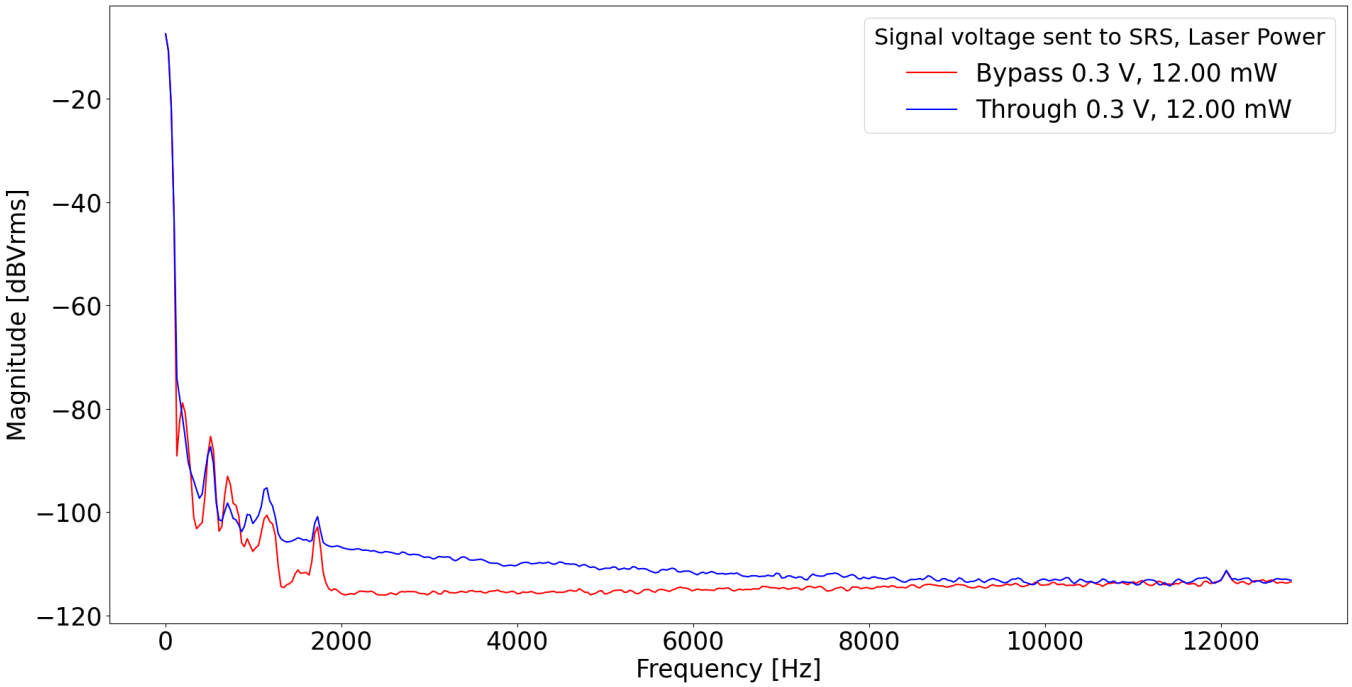

Figure 5.3: Signal spectrum for light (1278.76 nm) passing through as well as bypassing the sample at 2K

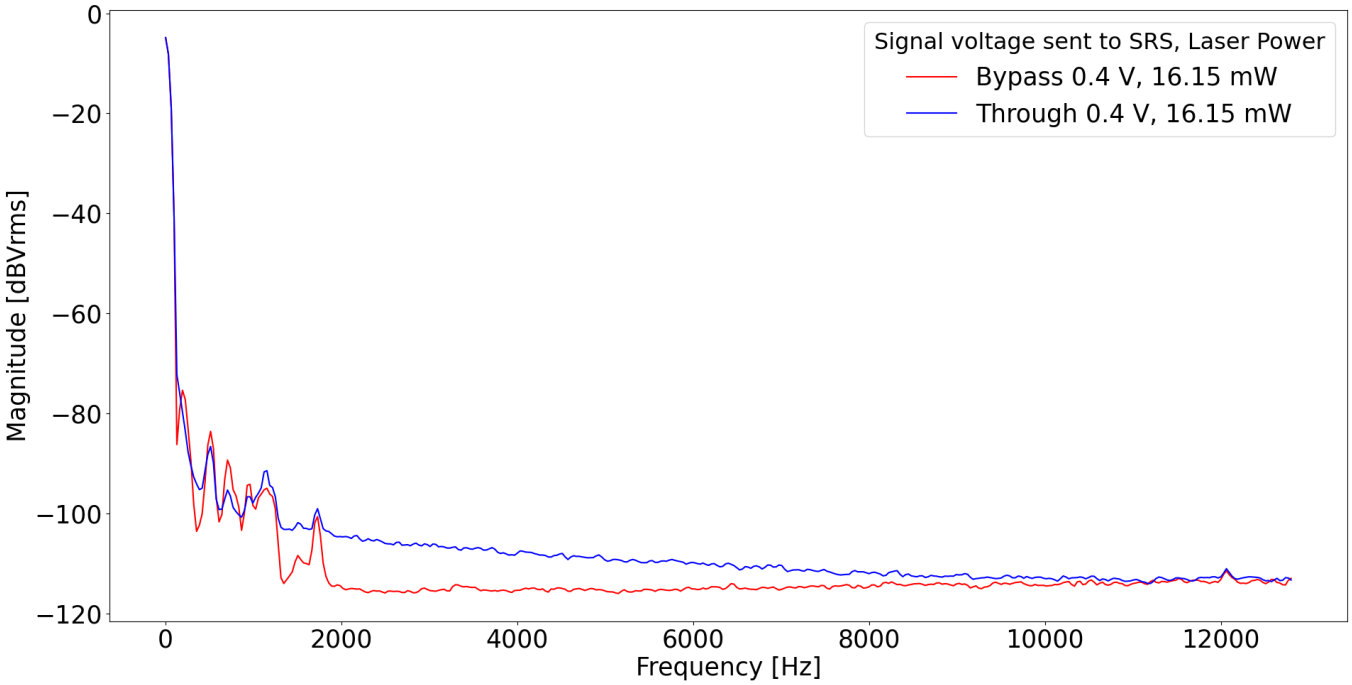

Figure 5.4: Signal spectrum for light (1278.76 nm) passing through as well as bypassing the sample at 2K

Appendix B: Power dependence of the difference between bypass and through sample

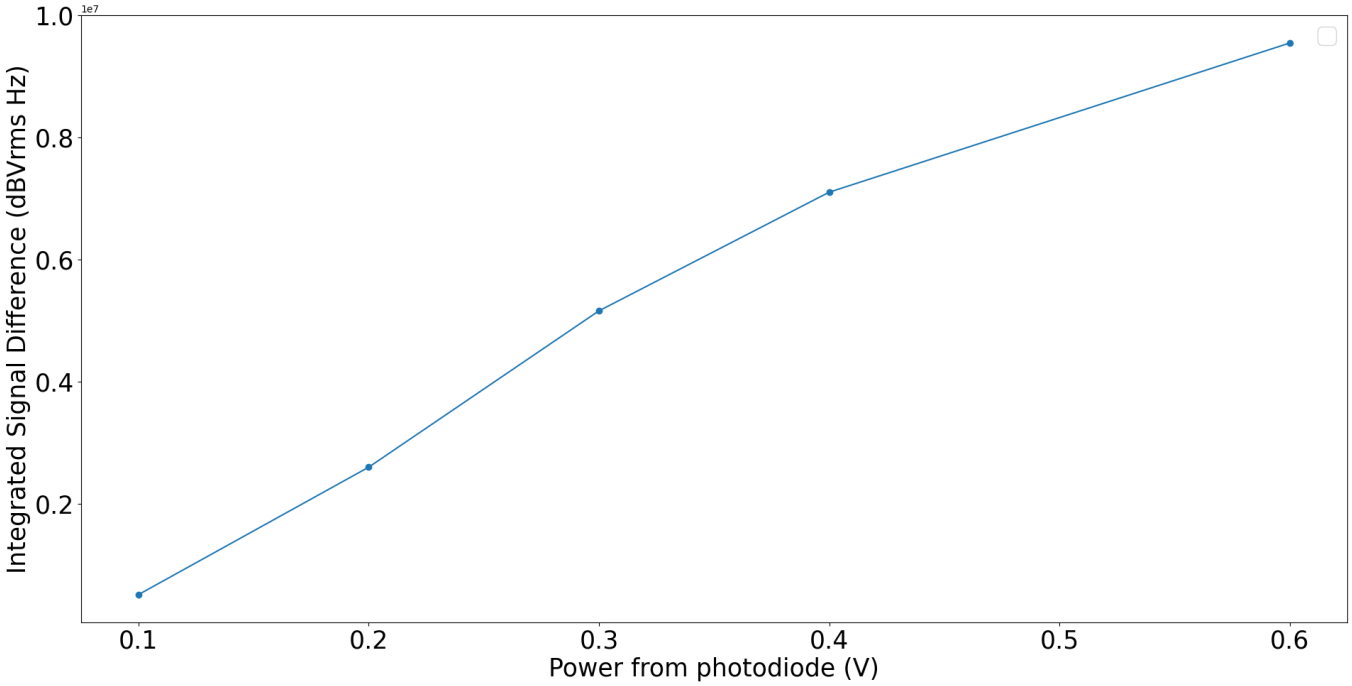

Figure 5.5: Integrated 1278.76 nm signals from Fig. 4.6 for different powers

Bibliography

[1] Kim Eun-jin. *SK Telecom Develops QKD Technology for Enterprises with No Dedicated Networks*. Apr. 2021. URL: http://www.businesskorea.co.kr/news/articleView.html?idxno=64188.

[2] Carmem M. Gilardoni. "Optically addressable spins in silicon carbide and related 2D materials: the role of symmetry and spin-orbit coupling". University of Groningen, 2021.

[3] Gary Wolfowicz et al. "Vanadium spin qubits as telecom quantum emitters in silicon carbide". In: *Science Advances* 6 (18 Apr. 2020). ISSN: 23752548. DOI: 10.1126/sciadv.aaz1192.

[4] Mark Fox. *Optical Properties of Solids*. 2nd ed. Oxford University Press, 2010. ISBN: 978–0–19–957336–3.

[5] Andrei Tokmakoff. *Time-Dependant Quantum Mechanics and Spectroscopy*. 2014.

[6] Benedikt Tissot and Guido Burkard. "Hyperfine Structure of Transition Metal Defects in SiC". In: (Apr. 2021). DOI: 10.1103/PhysRevB.104.064102. URL: http://arxiv.org/abs/2104.12351%20http://dx.doi.org/10.1103/PhysRevB.104.064102.

[7] Abraham Nitzan. *Chemical Dynamics in Condensed Phases*. 1st ed. Oxford University Press, 2006. ISBN: 978–0–19–852979–8.

[8] Russel Caflisch. *Random Walks with Gaussian Steps*. 2003. URL: https://www.math.ucla.edu/~caflisch/181.1.03f/.

[9] *Operating Manual and Programming Reference Model SR785 Dynamic Signal Analyzer*. Mar. 2017. URL: www.thinkSRS.com.

[10] Tibor Grasser. *Noise in nanoscale semiconductor devices*. Springer International Publishing, Apr. 2020, pp. 1–729. ISBN: 9783030375003. DOI: 10.1007/978-3-030-37500-3.